

Torsional vibrations in truck powertrains with dual mass flywheel having piecewise linear stiffness

Lina Wramner

Department of Mechanics and Maritime Sciences at Chalmers University of Technology and Volvo Group Trucks Technology, Gothenburg, Sweden

Summary. The vehicle industry faces big challenges when it comes to reducing the emissions of heavy vehicles. In order to cope with the increasing demand for efficient, low emission vehicles, the trend within the industry is to down-size and down-speed the engines. These measures lead to higher torsional vibrations in the powertrain and therefore there is also an increasing need for efficient reduction of torsional vibrations. One way to reduce the vibration is to use a dual mass flywheel. A dual mass flywheel consists of two flywheels connected by a torsional spring package. The spring package should have low stiffness but must also cope with very high torques. Therefore the dual mass flywheels are often designed so that they have a piecewise linear relationship between torque and wind-up angle. A full powertrain model has been used with realistic engine load in order to evaluate how the piecewise linear design affects the vibrations in the powertrain. Simulations have been performed in frequency domain and time domain and evaluation is done both with respect to mode shapes and frequencies and computed steady-state vibration amplitudes. In the linear region, there is a frequency shift for a problematic resonance mode that leads to significant decrease in vibration amplitude at low engine speeds. In non-linear regions, a resonance mode corresponding to half the main exciting frequency from the engine can be excited, leading to high vibration amplitudes. The frequency of this mode and the extent to which it is excited depends on the engine torque and highest amplitudes are not always obtained at the highest load.

Background

In typical truck powertrains, there is usually a torsional resonance that can be excited at low engine speeds. Truck manufacturers have learnt to deal with this resonance by using for example damping in the clutch, but the current development within the industry has led to an increasing need for better technology. The truck manufacturers face big challenges when it comes to reducing the emissions of heavy vehicles and in order to cope with the increasing demand for efficient, low emission vehicles, the trend is to down-size and down-speed the engines ([1, 2, 3]). This means that the engines will operate with higher vibratory load amplitudes at speeds closer to the resonance and this combined leads to an increasing need for efficient reduction of torsional vibrations. One way to reduce torsional vibrations is to use a dual mass flywheel. A dual mass flywheel consists of two flywheels connected by a low stiffness torsional spring package. By exchanging the standard flywheel with a dual mass flywheel, the resonance modes of the system are affected. The properties of the dual mass flywheel can be selected so that the problematic torsional resonance is not excited in the operating speed interval. This is very beneficial from a vibration point of view. Although dual mass flywheels have been successfully used for many years in smaller vehicles, the use in heavy vehicles is not standard and there is a need to better understand the torsional behaviour of the powertrain in heavy vehicles when a dual mass flywheel is used. A picture of a typical truck powertrain is shown to the left in Figure 1 and to the right is a schematic picture.

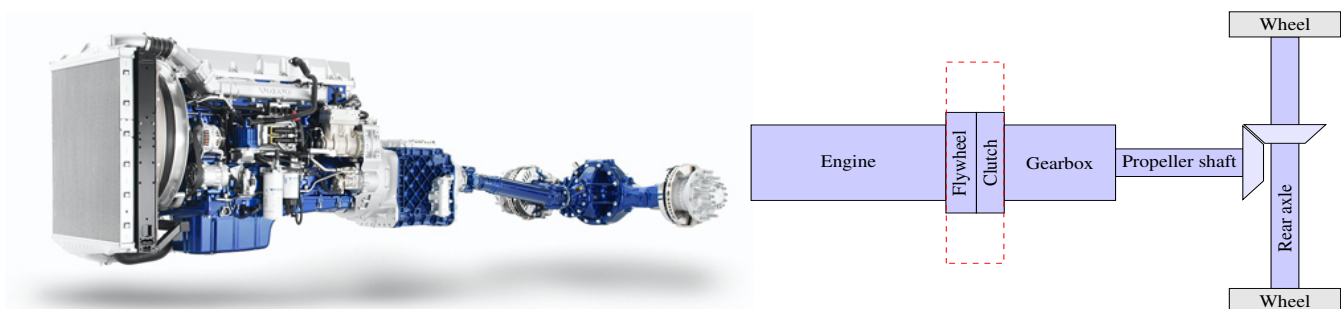


Figure 1: Truck powertrain, source: AB Volvo (left) and schematic picture of powertrain (right)

Objectives

Design limits on the dual mass flywheels make it difficult to design them in such a way that the spring package between the primary and secondary flywheel has sufficiently low stiffness at the same time as it can cope with very high torques. Therefore, it is often necessary to have higher stiffness at higher torques and hence a non-linear torque-angular displacement relationship between the primary and secondary flywheel. A common way to obtain this is by having a two-step stiffness as is illustrated in Figure 2. Here $\Delta\varphi$ represents wind-up angle, i.e. the angular displacement difference between secondary and primary flywheels. The values of the stiffness change angle θ , the primary stiffness k and the secondary stiffness $k + b$ will affect the torsional vibrations. The objective of this work is to understand how resonance modes and frequencies of the powertrain are affected when the standard flywheel and clutch are exchanged for a dual mass flywheel with piecewise

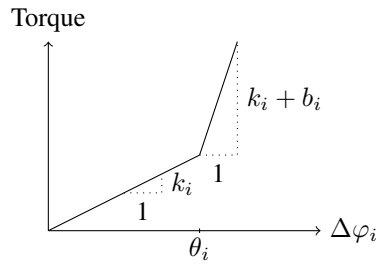


Figure 2: Piecewise linear torque-angular displacement relationship

linear relationship between wind-up angle and torque and how the torsional vibrations in the powertrain are affected at different engine speeds and load levels.

Conventional truck drivelines are fairly linear with respect to torsional vibrations and traditional evaluation methods within the industry usually involve harmonic response analyses at engine full load and consideration of the linear resonance frequencies. Care is taken to avoid resonances with frequencies that correspond to the main exciting frequency from the engine. For non-linear systems more sophisticated evaluation methods are needed and an additional objective of this work is to develop efficient methods for fast and accurate evaluation of torsional vibrations with non-linear models.

Methodology

The analysed powertrains are modelled with a set of discrete torsional elements, describing torsional properties of all functional components from engine to ground. Linear discrete torsional elements are used for all components but the dual mass flywheel. Each linear element is comprised of a gear ratio r_i , a linear spring with constant stiffness k_i in parallel with a viscous damper c_i and followed by rotating mass with constant moment of inertia j_i . This is illustrated in Figure 3. The angular displacement of j_i is denoted φ_i . The angular displacement before the gear ratio r_i is denoted φ_{i-1} . This

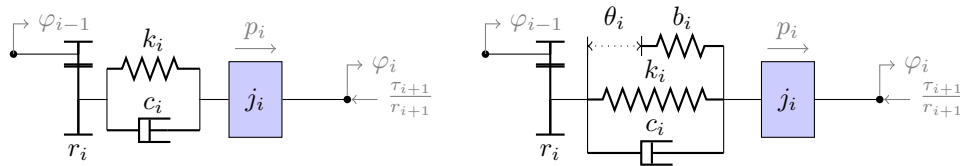


Figure 3: Linear discrete torsional element (left) and non-linear discrete torsional two-step stiffness element (right)

means that the angular elongation of spring k_i , $\Delta\varphi_i$ is given by $\Delta\varphi_i = \varphi_i - \frac{\varphi_{i-1}}{r_i}$. Let p_i denote an external torque on the moment of inertia j_i and $-\frac{\tau_{i+1}}{r_{i+1}}$ the torque from a subsequent element acting on j_i . The equation of motion for element i is

$$k_i \Delta\varphi_i + c_i \Delta\dot{\varphi}_i + \frac{\tau_{i+1}}{r_{i+1}} + j_i \ddot{\varphi}_i = p_i. \quad (1)$$

For the case with linear elements in series Equation (1) becomes

$$k_i \Delta\varphi_i + c_i \Delta\dot{\varphi}_i - \frac{k_{i+1} \Delta\varphi_{i+1} + c_{i+1} \Delta\dot{\varphi}_{i+1}}{r_{i+1}} + j_i \ddot{\varphi}_i = p_i. \quad (2)$$

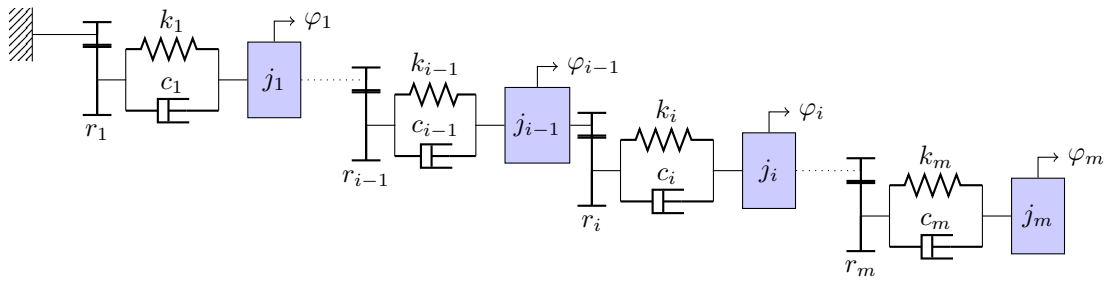
The two-step stiffness element used to model the springs in the dual mass flywheel with a piecewise linear torque-displacement relationship is illustrated to the right in Figure 3. The wind-up angle of the spring is denoted by $\Delta\varphi_i$ and at a certain wind-up angle θ_i , the stiffness changes from k_i to $k_i + b_i$. This means that the stiffness of the spring is characterized by k_i , θ_i and b_i . The equation of motion for the two-step stiffness element will be similar to that of the linear element in Equation (1) but with one extra term accounting for the impact of the additional stiffness for wind-up angles above θ_i .

$$k_i \Delta\varphi_i + b_i (\Delta\varphi_i - \theta_i) H(\Delta\varphi_i - \theta_i) + c_i \Delta\dot{\varphi}_i + \frac{\tau_{i+1}}{r_{i+1}} + j_i \ddot{\varphi}_i = p_i \quad (3)$$

$H(x)$ is the Heaviside step function, which is zero for values of x below zero and otherwise one.

In Figure 4, a schematic picture of the system used in the computational models of the truck powertrain is shown. The first element will be assumed to be connected to ground, which means that $\Delta\varphi_1 = \varphi_1$. Since powertrains are free at front end, the k_1 and c_1 values will be zero. For the last element m , there is no subsequent element and hence no torque contribution from a connecting element. The equation of motion will then be reduced to

$$k_m \Delta\varphi_m + c_m \Delta\dot{\varphi}_m + j_m \ddot{\varphi}_m = p_m. \quad (4)$$


 Figure 4: System with m discrete elements

The equations of motions for a complete linear system can be expressed on matrix form as

$$K\vec{\varphi} + C\dot{\vec{\varphi}} + J\ddot{\vec{\varphi}} = \vec{p}. \quad (5)$$

The angular displacement vector $\vec{\varphi} = [\varphi_1, \varphi_2, \dots, \varphi_m]^T$ and the external torque vector $\vec{p} = [p_1, p_2, \dots, p_m]^T$. The square matrices J , K and C are:

$$J = \begin{bmatrix} j_1 & 0 & \dots & 0 \\ 0 & j_2 & \dots & \vdots \\ \vdots & \vdots & \ddots & 0 \\ 0 & \dots & 0 & j_m \end{bmatrix} \quad K = \begin{bmatrix} k_1 + \frac{k_2}{r_2^2} & -\frac{k_2}{r_2} & 0 & \dots & 0 \\ -\frac{k_2}{r_2} & k_2 + \frac{k_3}{r_3^2} & -\frac{k_3}{r_3} & \ddots & \vdots \\ 0 & -\frac{k_3}{r_3} & k_3 + \frac{k_4}{r_4^2} & \ddots & 0 \\ \vdots & \ddots & \ddots & \ddots & -\frac{k_m}{r_m} \\ 0 & \dots & 0 & -\frac{k_m}{r_m} & k_m \end{bmatrix} \quad C = \begin{bmatrix} c_1 + \frac{c_2}{r_2} & -\frac{c_2}{r_2} & 0 & \dots & 0 \\ -\frac{c_2}{r_2} & c_2 + \frac{c_3}{r_3} & -\frac{c_3}{r_3} & \ddots & \vdots \\ 0 & -\frac{c_3}{r_3} & c_3 + \frac{c_4}{r_4} & \ddots & 0 \\ \vdots & \ddots & \ddots & \ddots & -\frac{c_m}{r_m} \\ 0 & \dots & 0 & -\frac{c_m}{r_m} & c_m \end{bmatrix} \quad (6)$$

When analysing the dual mass flywheel with two-step stiffness characteristics, the equations of motion will get one additional term, $\vec{f}(\vec{\varphi})$, describing the contribution from the increase in stiffness at higher wind-up angles which gives

$$K\vec{\varphi} + C\dot{\vec{\varphi}} + J\ddot{\vec{\varphi}} = \vec{p} - \vec{f}(\vec{\varphi}). \quad (7)$$

The elements in \vec{f} are zero, except at index $s-1$ and s , where s corresponds to the index of the secondary mass in the dual mass flywheel. From (3) follows that:

$$\begin{aligned} f_{s-1} &= -\frac{b_s}{r_s} H(\Delta\varphi_s - \theta_s) \\ f_s &= b_s H(\Delta\varphi_s - \theta_s) \end{aligned} \quad (8)$$

Computational methods

Only steady-state solutions will be considered and results are obtained both with time-domain simulations using Newmark's method and from harmonic balance method based simulations. The harmonic balance method is also used to find non-linear normal modes of the system, by using arc-length continuation scheme ([4]) starting from the linear resonance modes. Only the harmonic balance procedure will be outlined here. Consider models comprised of a series of linear elements combined with one non linear element as is illustrated in Figure 5. Assume that there exists a steady-state solution for a given periodic

load $\vec{p}(t) = \sum_{n=0}^N \vec{p}_n e^{i\frac{n}{2}\omega t}$. The torque from the non-linear stiffness and damping on inertia element s will be denoted by τ

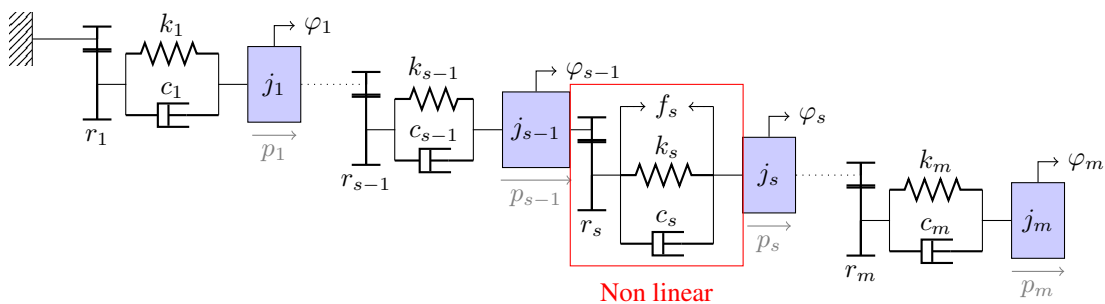


Figure 5: Model with one nonlinear element

(skipping the index s). Assume also that τ can be accurately described with a Fourier series with M components such that

$$\tau(t) = \sum_{n=0}^M \hat{\tau}_n e^{i\frac{n}{2}\omega t}. \quad (9)$$

We can then use the harmonic response method to find the corresponding steady-state solution to the linear submodel comprised of element 1 to $s - 1$, as shown on the left side of the dashed line in Figure 6. The applied load will then be

$$\vec{p}_{left}(t) = \sum_{n=0}^N \vec{\hat{p}}_{n(left)} e^{i\frac{n}{2}\omega t} + \sum_{n=0}^M \vec{\hat{\tau}}_{n(left)} e^{i\frac{n}{2}\omega t}. \quad (10)$$

Here, the vectors $\vec{\hat{\tau}}_{n(left)}$ and $\vec{\hat{p}}_{n(left)}$ of length $s - 1$ are given by

$$\vec{\hat{\tau}}_{n(left)} = [0, 0, \dots, 0, -\hat{\tau}_n]^T \text{ and } \vec{\hat{p}}_{n(left)} = [\hat{p}_{1,n}, \hat{p}_{2,n}, \dots, \hat{p}_{s-1,n}]^T. \quad (11)$$

Similarly we can find the corresponding steady-state solution of the rightmost submodel in Figure 6 by using the load

$$\vec{p}_{right}(t) = \sum_{n=0}^N \vec{\hat{p}}_{n(right)} e^{i\frac{n}{2}\omega t} + \sum_{n=0}^M \vec{\hat{\tau}}_{n(right)} e^{i\frac{n}{2}\omega t}. \quad (12)$$

The vectors $\vec{\hat{\tau}}_{n(right)}$ and $\vec{\hat{p}}_{n(right)}$ of length $m - s + 1$ are given by

$$\vec{\hat{\tau}}_{n(right)} = [\hat{\tau}_n, 0, 0, \dots, 0]^T \text{ and } \vec{\hat{p}}_{n(right)} = [\hat{p}_{s,n}, \hat{p}_{s+1,n}, \dots, \hat{p}_{m,n}]^T. \quad (13)$$

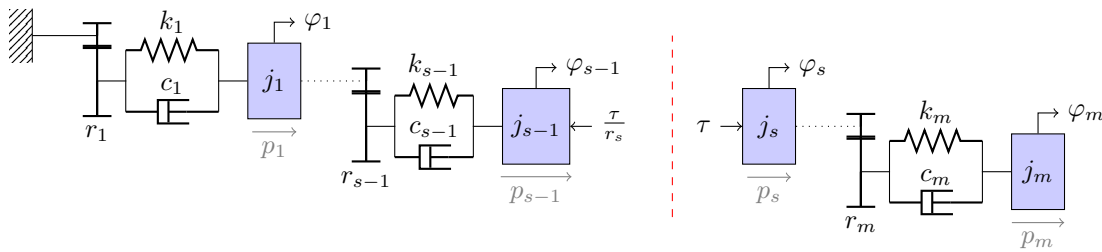


Figure 6: Separated model

From the harmonic response calculations of the left and right side we obtain values for the torsional displacements at the rightmost side of left submodel and leftmost side of right submodel, denoted, $\varphi_{s-1}^{(left)}$ and $\varphi_s^{(right)}$ respectively. This means that the relative displacement between inertia element $s - 1$ and s in the full model in Figure 5 is given by

$$\Delta\varphi_s(t) = \varphi_s^{(right)}(t) - \frac{\varphi_{s-1}^{(left)}}{r_s}(t) + \delta = \varphi_s(t) - \frac{\varphi_{s-1}}{r_s}(t). \quad (14)$$

Here δ is a constant offset value. The relative velocity is given by $\Delta\dot{\varphi}_s = \dot{\varphi}_s - \frac{\dot{\varphi}_{s-1}}{r_s}$. Based on the non linear functions of the stiffness and damping in element s , the torque can be calculated for different values of δ . If we know the mean torque per cycle an iterative procedure can be used to find the value of δ . Once we have δ , the torque $\vec{\tau}$ corresponding to the relative displacements can be calculated. Finding the solution is then a matter of minimizing the function

$$\vec{g} = \vec{\tau} - \vec{\tau}. \quad (15)$$

The efficiency of the algorithm can be improved further by reducing the linear systems to the left and right of the non-linearity.

Powertrain modelling

A typical truck powertrain is comprised of an engine, a flywheel, a clutch, a gearbox, a propeller shaft and a rear axle and wheels in series, as shown in Figure 1. Simulated torsional vibrations with such a typical driveline will be compared with corresponding results for a driveline where the flywheel and clutch in the red dashed box in the figure are exchanged for a dual mass flywheel and clutch. In the subsequent sections, the modelling details of the powertrain components are explained.

Engine

A six cylinder, 4-stroke, 13-litre engine is modelled. The crankshaft is divided into 8 discrete rotational masses according to Figure 7. The big ends of the connecting rods rotate with the crankshaft, whereas the small ends follow the vertical piston motion. Therefore the part of the connecting rods contributing with moment of inertia is estimated and the resulting moment of inertia is added to the corresponding crankshaft discrete mass. The moment of inertia of the damper housing

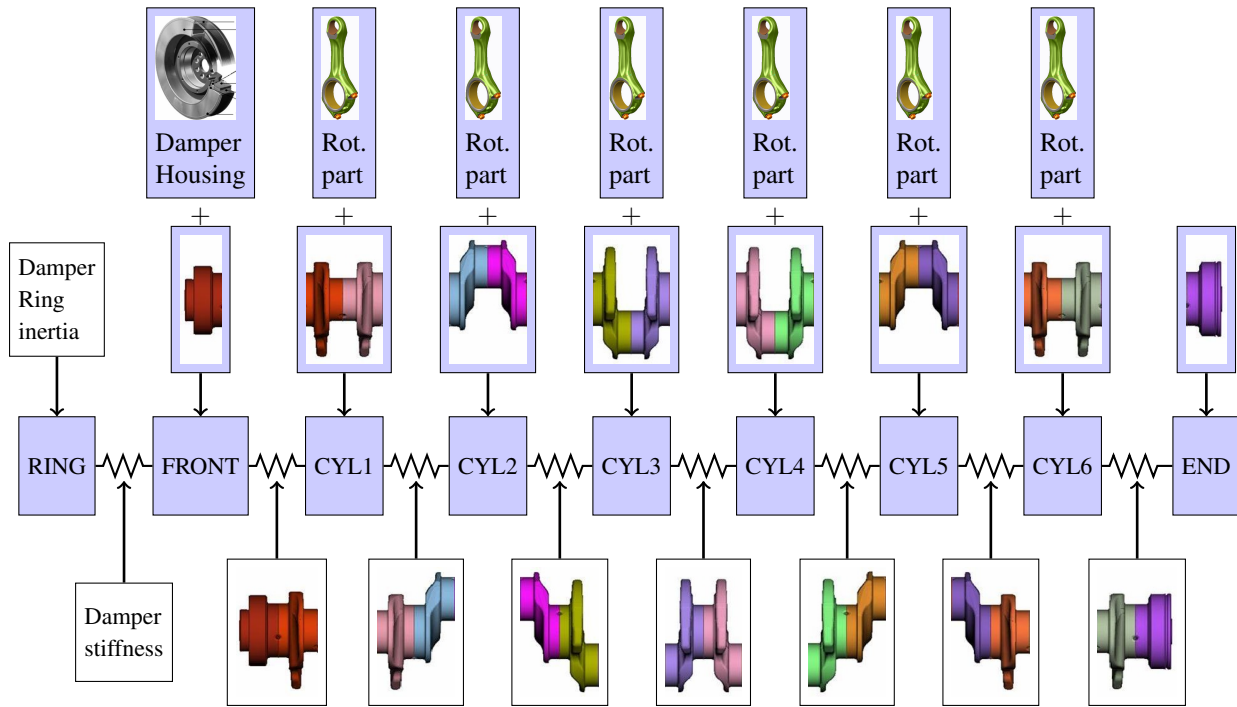


Figure 7: Discrete Engine Model

and bolts are added to the mass corresponding to the frontmost part of the crankshaft and this mass is connected with a spring to a discrete mass representing the damper ring. The spring stiffness represents the stiffness of the fluid between the damper ring and housing.

It is assumed that the load at each cylinder, comprising load coming from the cylinder pressure and load from the oscillating mass (piston mass) is periodic with period 720 degrees. The load $P_{CYL1}(t)$ at first cylinder will be expressed as

$$P_{CYL1}(t) = \text{Real}\left(\sum_{n=0}^{24} A_n e^{i\frac{n}{2}\omega t}\right). \quad (16)$$

Here ω denotes the angular velocity of the crankshaft and A_n are complex numbers. The load at the other cylinders will be assumed to be equivalent, but shifted in phase. For a phase difference between cylinder k and 1 equal to β_k we have

$$P_{CYLk}(t) = \text{Real}\left(\sum_{n=0}^{24} A_n e^{i\frac{n}{2}\omega t - i\frac{n}{2}\beta_k}\right). \quad (17)$$

The phase differences β_k for $k = 1$ to 6 are 0 degrees, 480 degrees, 240 degrees, 600 degrees, 120 degrees and 360 degrees respectively. In future engines it is expected that the torque will be higher at lower engine speeds. Therefore three different sets of load data, Load A, B and C will be analysed. Load B and C are obtained from Load A, by shifting the cylinder pressure data for engine speeds of 1000 rpm and below down by 50 rpm and 100 rpm respectively. This is illustrated to the left in Figure 8, where the resulting mean torque is shown. To the right in Figure 8, the calculated torque from Load A just before the flywheel is shown for the conventional powertrain and some engine speeds. Note that for a different powertrain model this calculated torque would be different.

Flywheel, clutch and dual mass flywheel

In a conventional truck powertrain, the flywheel and clutch have very large moments of inertia. Since only steady-state vibrations will be considered in this work, it will be assumed that flywheel and clutch are rigidly connected. The clutch damper consists of weak torsional springs that are located near the clutch hub and connected to the gearbox input shaft with very small moment of inertia in between. In Figure 9, it is shown to the left how a standard flywheel/clutch configuration is modelled. There is also some damping in the spring which will be modelled as viscous. A dual mass flywheel consists of a primary and secondary flywheel which are connected via a low stiffness torsional spring package. The clutch is connected to the secondary flywheel. This clutch could be fairly rigid or could have a clutch damper included. In this work, the clutch used with the dual mass flywheel will be considered rigid. In Figure 9 it is shown to the right how a dual mass flywheel configuration is modelled.

Gearbox

The gearbox is modelled with five discrete rotational masses as shown in Figure 10. The data for each gearbox gear will be different, since the gear wheels and shafts will rotate with different speeds and the torque paths will be different for

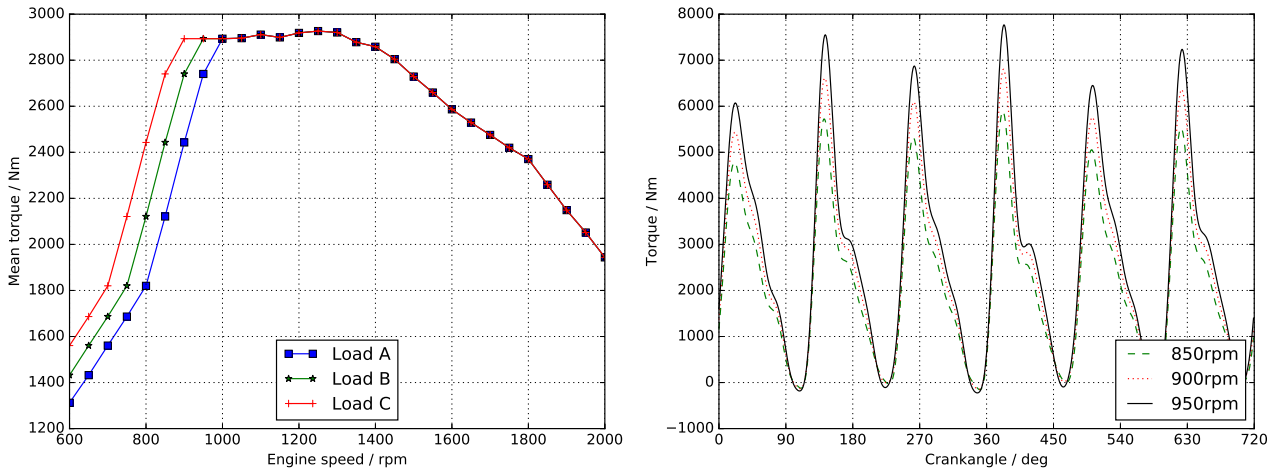


Figure 8: Engine mean output torque (left) and torque before flywheel in conventional powertrain with Load A (right)



Figure 9: Discrete models of standard flywheel clutch configuration and with dual mass flywheel respectively

different gearbox gears. Figure 10 illustrates how the different parts of the gearbox are lumped to the five discrete elements. The small picture to the right defines the parts of the moment of inertia on each side of the gearwheels and in the left picture it is shown how their contributions are added together.

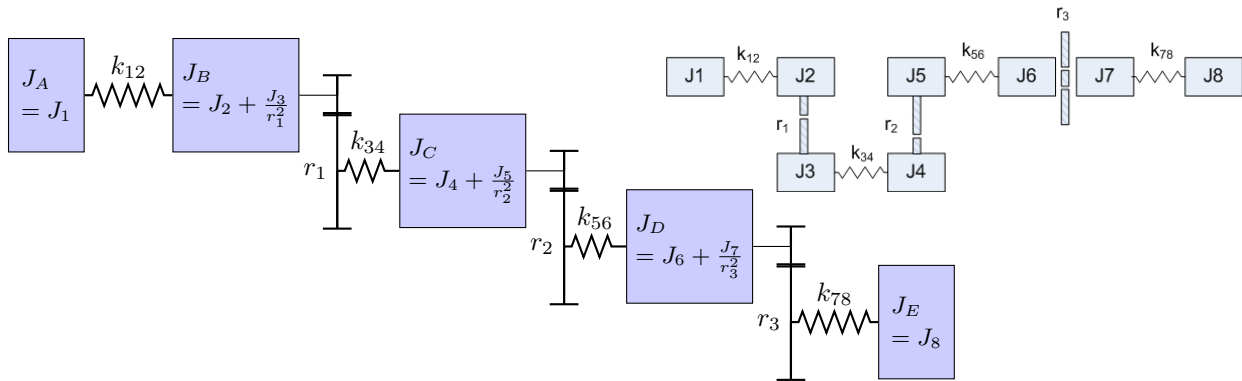


Figure 10: Discrete model of the gearbox

Rear driveline

The parts of the powertrain rear of the gearbox are modelled with five discrete elements, as illustrated in Figure 11.

For a tyre radius ρ , wheel angular acceleration $\dot{\omega}_{wheels}$, vehicle acceleration a and vehicle mass m we have that the torque from ground on the wheels equals

$$T = m a \rho = m \dot{\omega}_{wheels} \rho^2. \quad (18)$$

So by modelling the vehicle as a rotating mass with moment of inertia $I = m \rho^2$ and angular acceleration $\dot{\omega}_{wheels}$, the effects of vehicle acceleration will be included in the model. Since the steady-state results are the focus of this study, a negative load corresponding to the mean load from the engine times the cumulated gear ratio will be applied at the rear end of the model, corresponding to aerodynamic and rolling resistance. This will ensure that the mean engine speed will be fixed in the simulation.

Model data

The data used in simulations are representative for a 13-litre heavy duty premium truck. In Table 1, the data used in the simulations for the conventional powertrain are shown at the top and the additional data used for the dual mass flywheel at the bottom. The stiffness shown is that for the primary stiffness, k , which is constant in all simulations. The stiffness change angle θ used in the non-linear simulation is 0.24 radians and the secondary stiffness will be $k(1 + \alpha)$ where α is a parameter that is varied.

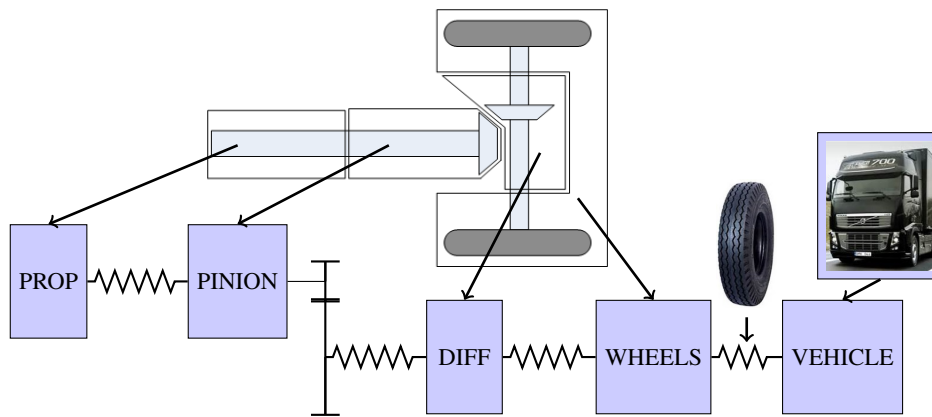


Figure 11: Discrete model of propeller shaft, rear axle, wheels and vehicle

		Gear ratio	Torsional stiffness/ Nm/rad	Viscous damping/ Nms/rad	Moment of inertia/ kgm ²
Data for conventional powertrain					
1	RING	1	0		0.1837
2	FRONT	1	142835	100	0.1182
3	CYL1	1	4440282		0.1325
4	CYL2	1	3088151		0.1065
5	CYL3	1	3088421		0.1325
6	CYL4	1	3119504		0.1325
7	CYL5	1	3094713		0.1065
8	CYL6	1	3109410		0.1328
9	END	1	4588336		0.1182
10	FLYWHEEL	1	∞		1.3063
11	CLUTCH	1	∞		1.3343
12	HUB	1	20795	49.5	0.0600
13	CONNECTION	1	∞		0.0568
14	INPUT SHAFT	1	197572		0.0951
15	COUNTER SHAFT	0.881	7028988		0.2910
16	MAIN SHAFT	0.9105	561151		0.3617
17	OUTPUT SHAFT	1	1391923		0.0217
18	PROP	1	∞		0.1972
19	PINION	1	161751		0.1461
20	DIFF	2.66	∞		2.1841
21	WHEELS	1	208524		10.4673
22	VEHICLE	1	1392000	300	11436.4000
Data for dual mass flywheel and clutch					
10	PRIMARY FLYWHEEL	1	∞		1.8000
11	SECONDARY FLYWHEEL	1	10890	49.5	1.8000
12	HUB	1	∞		0.0600

Table 1: Model data

Results

Torsional vibrations at steady state are evaluated for a typical truck driveline with conventional flywheel based on the data in Table 1 and load corresponding to engine full load. These results are compared with the corresponding results for the model when the flywheel and clutch are exchanged for the dual mass flywheel and clutch. In Figure 12, the first linear resonance modes with the driveline having a standard flywheel are shown with blue lines and the corresponding modes with the driveline having a dual mass flywheel are shown with red dashed lines. For visualisation purposes the angular displacement for each mode is multiplied with the cumulated gear ratio. The second mode is often problematic for gearboxes in standard drivelines. In six-cylinder four stroke engines there are three cylinders firing for each crankshaft revolution. This means that the load will have a big oscillating component of a frequency corresponding to three times the crankshaft angular velocity, usually referred to as third engine order. At low engine speeds, the frequency of the second resonance mode is close to the third engine order which can lead to high vibration amplitudes. When a dual mass flywheel

is introduced, the frequency of the second mode is reduced. This indicates an improvement in torsional vibrations at low speeds and is in accordance with what is observed in simulations with linear models. The frequency of the third resonance mode in the driveline is only marginally affected by the dual mass flywheel. This mode is generally highly damped and not a big problem in conventional drivelines. The higher resonance modes are also affected by the dual mass flywheel and there is a risk of a higher mode causing problem at high engine speeds. These high engine speeds are not the focus of this study.

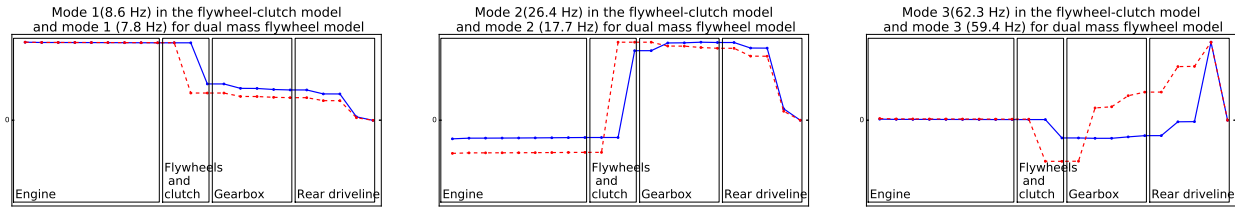


Figure 12: Resonance modes and frequencies

In Figure 13 the relative angle between the secondary and primary flywheel in the dual mass flywheel is shown for Load A at some different values of α . The red lines show the amplitude of the 3rd engine order vibration. The blue lines show the amplitude of the 1.5th engine order vibration. The green dashed lines show the difference between relative angle caused by the mean torque and the stiffness change angle, θ . The black lines show the maximum and minimum deviation from the equilibrium position. When the green dashed line is above both black lines, the vibrations occur in the primary stiffness region. When the green dashed line is below the black lines, the vibrations occur in the secondary stiffness region and when the green line is between the black lines, the vibrations occur in both regions.

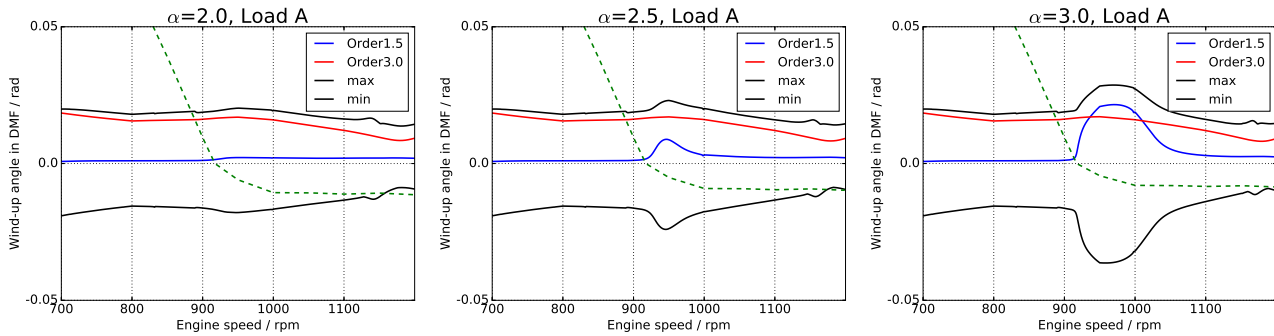


Figure 13: Dual mass flywheel wind-up angles for different α values

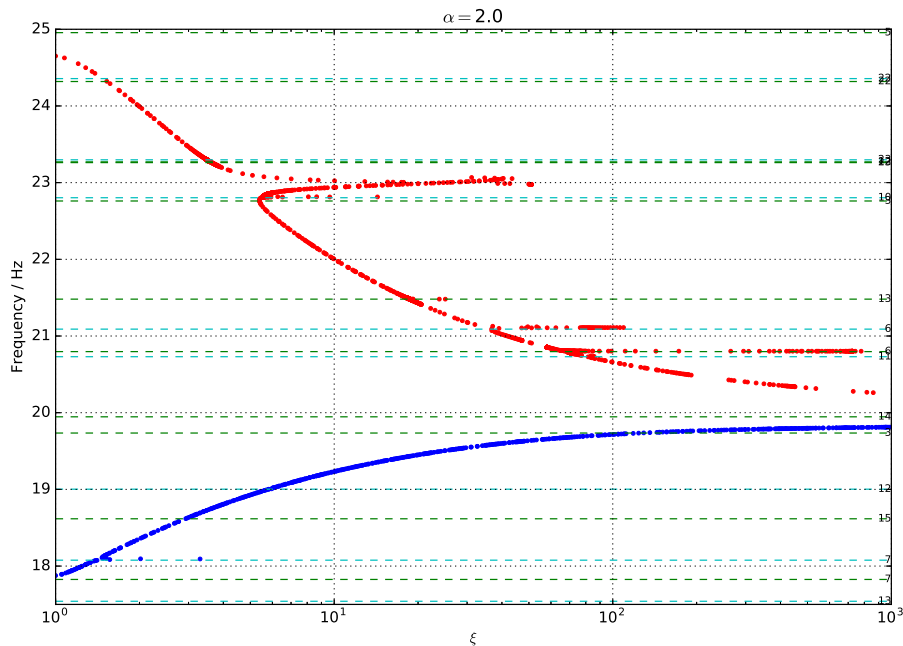
When α is increasing we can observe high vibration amplitudes at low engine speeds with a frequency corresponding to 1.5th engine order. The engine load for this frequency is relatively low and the high 1.5th engine order response is observed also for pure third engine order excitation so this is a consequence of the non-linearity in the dual mass flywheel.

The resonance frequency of the second driveline mode at the primary stiffness in the dual flywheel is 18 Hz and the corresponding frequency for the higher stiffness for $\alpha = 3$ is 27 Hz. This means that when vibrations occur in both the primary and secondary region of the dual mass flywheel we should expect a resonance with frequency somewhere in between these values, and it would show up as a 1.5th engine order vibration at engine speeds between 720 and 1080 rpm. At 720 rpm, the vibration is only in the linear primary stiffness region so here we would expect to see a resonance peak for engine order 1.5. This is the case for lower damping, but not with the used damping from Table 1.

Figure 14 shows the frequencies of some of the non-linear normal modes for the conservative system (no damping) corresponding to the powertrain model with $\alpha = 2.0$. The frequency shown in the plot is the lowest frequency of the system and there are significant vibration amplitudes for frequencies at multiples of the base frequency as well. The frequencies are shown as a function of parameter ξ , where ξ is defined as

$$\xi = \frac{E}{E_{nl}}. \quad (19)$$

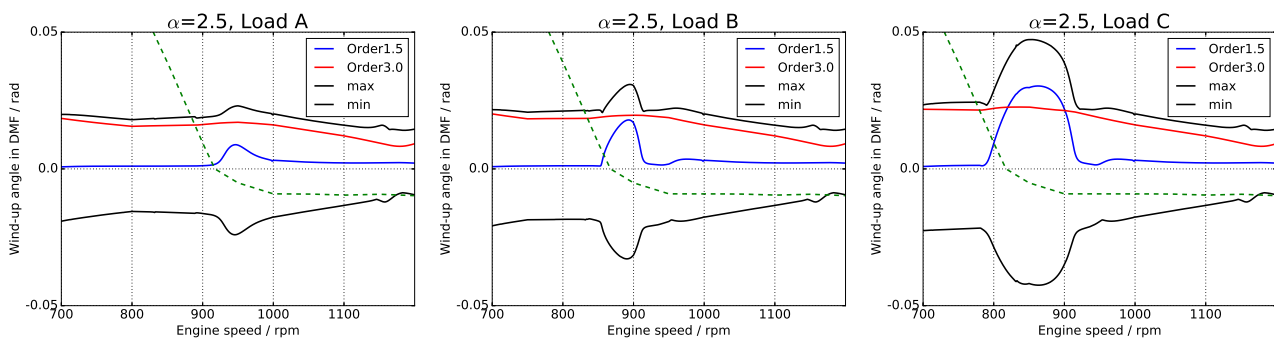
Here E denotes the total energy of the system and E_{nl} denotes the energy needed to enter the non-linear region. It has been seen that for fixed values of α and ξ the same frequencies are obtained independent of E and E_{nl} . This means that it is only necessary to analyse the non-linear normal modes for one value of the stiffness change angle θ . The blue dots show the non-linear normal modes obtained when the mean position is in the primary stiffness region of the dual mass flywheel. At $\xi = 1$ we have only vibrations in the linear region and the frequency equals that of the linear resonance mode. As the system energy and ξ increase a longer time is spent in the secondary stiffness region and hence the resonance frequency decreases. When the stiffness change angle θ decreases, E_{nl} decreases as well, which leads to an increase in ξ and a higher frequency. The red dots show the corresponding non-linear modes obtained when the mean position is in the secondary stiffness region of the dual mass flywheel. At $\xi = 1$ we have the linear resonance mode corresponding to the secondary


 Figure 14: Non-linear normal mode for $\alpha = 2.0$

stiffness. When ξ increases due to an increase in energy or decrease in the stiffness change angle θ , the time spent in the primary stiffness region also increases and we get a decrease in frequency. As ξ increases the branches following the linear resonance modes at primary and secondary stiffness approach the same frequency. In Figure 14 we can also see that at some frequencies we have horizontal branches where the frequency is constant as ξ increases. Here the frequency is close to a multiple of one of the linear resonances of the systems to the rear and front of the non-linearity (the factor shown with small figures to the right in Figure 14). As the energy increases the corresponding linear part of the oscillation increases as well. At some frequencies there are several stable solutions with different energy. Time-domain simulations also show that several different steady-state solutions can be obtained for the same engine load. This will be subject to future research in the project.

From Figure 14 we can deduce that an increase in mean load will lead to an increase in resonance frequency. An increase in load amplitude will lead to a higher resonance frequency if the wind-up angle due to the mean torque is in primary stiffness region and otherwise it will lead to a lower resonance frequency.

In Figure 15, the relative angle between the secondary and primary flywheel in the dual mass flywheel is shown for $\alpha = 2.5$ and Load A, B and C. The peak amplitudes occur at lower engine speeds for the higher load. This is contrary to what


 Figure 15: Dual mass flywheel wind-up angles for $\alpha = 2.5$ and Load A, B and C

is expected based on the previous conclusion that resonance frequency increases with load. The resonance frequency increases with increasing load, but how much the resonance is excited depends on how much of the time is spent in primary and secondary stiffness regions. For vibrations mainly in primary or mainly in secondary stiffness region, there will be low excitation of modes corresponding to 1.5th engine order and as the time spent in the two stiffness regions become more similar the 1.5th engine order excitation will increase.

So to conclude, high 1.5th engine order vibration amplitudes will be observed when mean load results in a wind-up angle in the dual mass flywheel close to the stiffness change angle and when the non-linear resonance frequency corresponds to half the main excitation frequency from the engine. This means that the worst vibration amplitudes do not necessarily occur at the highest load.

Conclusion and outlook

A mathematical model for simulation of torsional vibrations in heavy truck powertrain with dual mass flywheel with piecewise linear characteristics is proposed. The model comprises a set of discrete vibratory elements modelling powertrain with all functional components from engine to ground. The developed model is used to evaluate resonance modes and to predict torsional vibrations obtained at different operating points with realistic loads from the engine when a conventional flywheel is exchanged for a dual mass flywheel with piecewise linear characteristics.

In the linear region the results show a frequency shift for the problematic second powertrain resonance mode that leads to a decrease in vibration amplitude at low engine speeds. In non-linear regions, the results show that a resonance mode with frequency corresponding to half the main exciting frequency from the engine can be excited at low engine speeds, leading to high vibration amplitudes. The frequency of the resonance mode depends both on the average torque and on the torque amplitude. A higher average torque results in a higher resonance frequency. If the wind-up angle caused by the mean torque is in the secondary stiffness region of the dual mass flywheel, a higher torque amplitude will lead to a lower resonance frequency, otherwise it will lead to a higher resonance frequency. Moreover, the extent to which the resonance mode is excited depends on the engine torque and the highest amplitudes are not always obtained at the highest load.

Investigation of the non-linear normal modes shows that at some frequencies there are several stable solutions with different energy. Time-domain simulations also show that several different steady-state solutions can be obtained for the same engine load. This complicates the evaluation since depending on the initial conditions used in the simulation different steady-state vibration amplitudes are obtained. All this shows that sophisticated evaluation methods are needed in order to evaluate the impact on torsional vibrations of non-linear components in a large range of engine speeds and load levels.

The stability of the solutions and how to find and assess different solutions will be subject to future research in the project. It will also be further studied how non-linearities in combination with realistic engine load can lead to high excitation of different resonance modes and how progressive stiffness in dual mass flywheels should be designed in order to minimise torsional vibration problems in truck drivelines.

Acknowledgements

This research is part of the doctoral project "Reduced vibration transmissions - reduced energy consumption and environmental impacts together with an increased competitiveness" which is funded by the Swedish Energy Agency (project No. 42100-1). My supervisors Viktor Berbyuk, Håkan Johansson and Anders Hedman are appreciated for their fruitful comments that improved the quality of this paper.

References

- [1] Arndt Ihleman. "Solving the Powertrain Puzzle". In: *Schaeffler Technologies GmbH & Co. KG* (2014), pp. 172–186. DOI: 10.1007/978-3-658-06430-3. URL: <http://link.springer.com/10.1007/978-3-658-06430-3>.
- [2] P. Kelly et al. "Dual mass flywheel as a means of attenuating rattle". In: *Tribology and Dynamics of Engine and Powertrain* (2010), pp. 857–877. DOI: 10.1533/9781845699932.2.857. URL: <http://linkinghub.elsevier.com/retrieve/pii/B9781845693619500284>.
- [3] Georg Johann Meingaßner, Hermann Pflaum, and Karsten Stahl. "Innovative Torsional Vibration Reduction Devices - Vehicle-Related Design and Component Strength Analysis". In: *SAE International Journal of Passenger Cars - Mechanical Systems* 7.4 (2014), pp. 1392–1403. ISSN: 1946-4002. DOI: 10.4271/2014-01-2862. URL: <http://www.scopus.com/inward/record.url?eid=2-s2.0-84946918178%7B%5C%7DpartnerID=tZ0tx3y1>.
- [4] M. Peeters et al. "Nonlinear normal modes, Part II: Toward a practical computation using numerical continuation techniques". In: *Mechanical Systems and Signal Processing* 23.1 (2009), pp. 195–216. ISSN: 08883270. DOI: 10.1016/j.ymssp.2008.04.003.